JOURNAL OF COMPUTATIONAL PHYSICS 86, 168–186 (1990)

A Numerical Algorithm to Study Internal Solitary Waves

CHARLES QUON AND HELMUTH SANDSTROM

Physical and Chemical Sciences, Department of Fisheries and Oceans, Bedford Institute of Oceanography, Dartmouth, Nova Scotia, Canada B2Y 4A2

Received February 26, 1988; revised February 27, 1989

This paper presents a finite difference method to solve two coupled, one-dimensional, nonlinear, dispersive, and non-dissipative partial differential equations. They describe the generation and propagation of internal solitary wave trains along the interface of an inviscid two-layer fluid over a variable bottom topography. Since the existence of solitary waves requires a balance between dispersion and nonlinear effects, great care has been taken to minimize the numerical dispersion which could otherwise overwhelm the mild analytic dispersion and thereby alter the shape and propagation characteristics of the solitary waves. Because the equations contain terms representing continuous forcing and arbitrary bottom topography, we can use the numerical algorithm presented here to study internal solitary waves in a natural fluid environment.

1. INTRODUCTION

In the past, many authors have studied numerically the interaction of two solitary waves of assumed forms. Others have studied the formation of solitary waves from an unbalanced initial condition for either the KdV or the MKdV equation. As an alternative, Chu *et al.* [3] studied numerically the so-called piston problem in a homogeneous fluid. High amplitude nonlinear waves were generated by injecting a uniform inflow at the boundary of a semi-infinite channel for a finite period of time. The propagation characteristics of these waves were then studied.

In this paper, we shall present a numerical algorithm to study the generation and propagation of internal solitary waves along the interface of a two layered fluid. The waves are forced by a time dependent barotropic flow over an abrupt change in bottom topography. Our model differs from the previous ones in two important aspects: 1. It is forced continuously by a time dependent function; 2. It has incorporated an arbitrary bottom topography. It is believed that the present study is among the first to investigate the generation, evolution, and propagation of solitary internal waves due to continuous forcing. Although the physical interpretation of the waves is of oceanographic origin, the method of solution is general.

2. THE PHYSICAL MODEL

An inviscid, incompressible, two-layer flow over topography (Fig. 1) is started from rest. In the state of rest, a thinner layer of fluid of constant depth r_1 and

0021-9991/90 $3.00

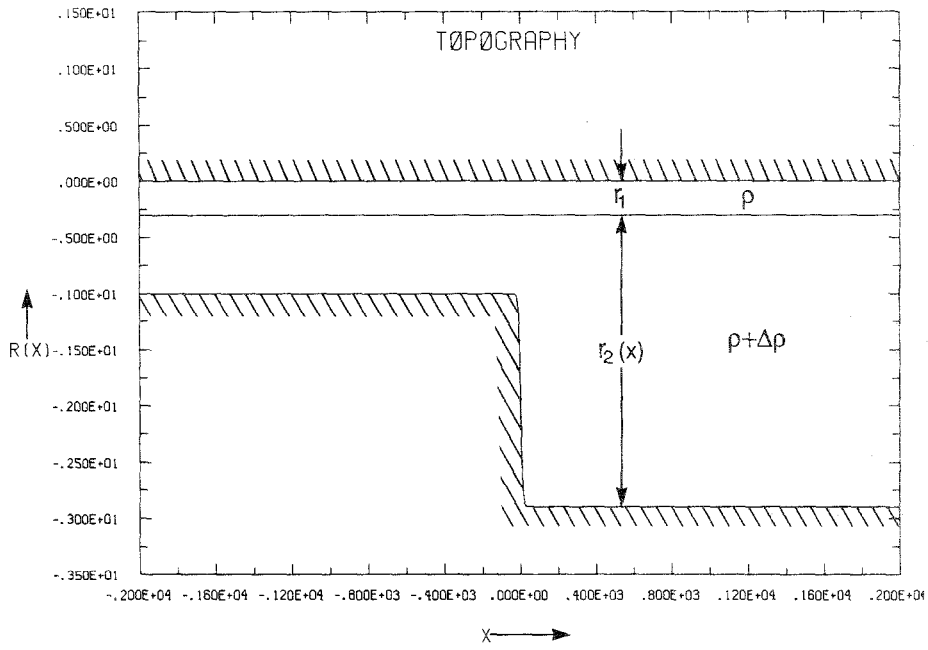

FIG. 1. The two-layered fluid system and step topography with smooth corner: $r(x) = 1/2[21.0 + 19.0 \tanh(x/10)]$.

density ρ lies over a deeper layer of constant density $(\rho + \Delta\rho)$ and of variable depth $r_2(x)$. The total depth of fluid is $r(x) = r_1 + r_2(x)$. The system is forced by an arbitrary, time-dependent, barotropic flow. The flow remains irrotational and the basic equations are formulated in terms of velocity potentials in the two layers, together with the kinematic and dynamic interface conditions. Free surface effects are eliminated by assuming that it is covered with a flat, rigid lid.

Following the procedure used by Whitham [14] for a single-layer fluid, the velocity potentials are expanded about the hydrostatic solution to include vertical acceleration (dispersion) effects to the first order. The expansion in the variable depth lower layer satisfies the bottom boundary condition. The expansions are substituted into the kinematic and dynamic interface conditions as in [14].

If the water depth on the shelf is used as characteristic length, L, $V = \sqrt{(\Delta\rho/\rho)\, gL}$ as the characteristic velocity, and L/V as the characteristic time, g being the earth's gravity, the dimensionless governing equations are [12]

$$\partial S/\partial t + S\,\partial A/\partial x + A\,\partial S/\partial x + \partial B/\partial x - \partial(S^2 U/r)/\partial x = 0 \tag{1}$$

$$\partial U/\partial t + \partial S/\partial x + C\,\partial U/\partial x + U\,\partial C/\partial x + 2DU\,\partial U/\partial x + U^2\,\partial D/\partial x - \partial(U^2 S/r)/\partial x - \partial^3(\sigma(x)\,U)/\partial x^2\,\partial t = 0 \tag{2}$$

$$A(U, x; t) = q(t)/r(x) - (r_1 - r_2(x))/r(x) \cdot U \tag{3a}$$

$$B(U, x; t) = -q(t)/r(x) + r_1 \cdot r_2(x)/r(x) \cdot U \tag{3b}$$

$$C(x, t) = q(t)/r(x) \tag{3c}$$

$$D(x) = (r_1 - r_2(x))/r(x) \tag{3d}$$

$$\sigma(x) = r_1 \cdot r_2(x)/3. \tag{3e}$$

In (1)–(3), $S(x, t)$ is the interfacial elevation, $U(x, t)$ is the current shear defined as the difference between mean velocities in the lower and upper layer, respectively, and $q(t)$ is the non-dimensional mass flux and is prescribed arbitrarily.

Equation (1) is derived from continuity and is exact. It contains cubic non-linear terms. In Eq. (2), the dynamic interface condition, non-linear terms are again retained to third order, but dispersive terms only to first order. Hence the physical model consists of a pair of coupled non-linear and weakly dispersive third-order equations.

If the amplitude of the forcing function, $q(t)$, remains suitably small (hydraulically sub-critical), the baroclinic disturbance originating at the abrupt change of topography propagates at finite speed towards $x = \pm\infty$. The boundary conditions can then be chosen as $S = U = 0$ at $|x| = \infty$.

3. The Numerical Method

Evolution equations similar to (1) and (2) have been solved numerically with pseudospectral methods [5, 7], and with finite difference methods [3, 4, 10, 11, 15, 16]. A collection of the earlier methods can be found in [13]. In this paper, we shall describe a two and one-half step predictor-corrector finite difference method. The essence of the method is as follows: (a) At time step $(n+1)$, we approximate S^{n+1} by S^* explicitly; (b) compute U^{n+1} implicitly in terms of S^*, S^n, and U^n; (c) correct S^{n+1} in terms of U^{n+1}, U^n, and S^n. This method is similar to that used in [11]. Since our physical model is nondissipative and only mildly dispersive, it is very important to control the numerical dissipation and dispersion due to truncation errors. If not, as we shall demonstrate later, they can distort severely the shape and propagation characteristics of these waves. We shall study these effects and propose procedures to control them.

The procedure can be symbolically written as

$$(\partial S/\partial t)^* + \overline{S^*}\,\partial A^n/\partial x + A^n\,\partial S^n/\partial x + \partial B^n/\partial x - \overline{S^*}[2U^n/r \cdot \partial S^n/\partial x + S^n\,\partial(U^n/r)/\partial x] = 0 \tag{4}$$

$$(\partial U/\partial t)^{n+1/2} + C^{n+1/2}\,\overline{\partial U/\partial x}^{n+1/2} + 2DU^n\,\overline{\partial U/\partial x}^{n+1/2} - (\partial^3(\sigma U)/\partial x^2\,\partial t)^{n+1/2} = \partial[(U^n)^2\,\overline{S^*}/r]/\partial x - (\partial\,\overline{S^*}/\partial x - U^n\,\partial C^{n+1/2}/\partial x - U^n)^2\,\partial D/\partial x \tag{5}$$

$$(\partial S/\partial t)^{n+1/2} + S^n\,\overline{\partial A/\partial x}^{n+1/2} + \bar{A}^{n+1/2}\,\partial S^n/\partial x + \overline{\partial B/\partial x}^{n+1/2} - \partial[(S^n)^2\,\bar{U}^{n+1/2}/r]/\partial x = 0. \tag{6}$$

In these equations, S^* approximates S^{n+1}, and $(\partial S/\partial t)^* = (S^* - S^n)/\Delta t$ approximates $(\partial S/\partial t)^{n+1/2} = (S^{n+1} - S^n)/\Delta t$; $\bar{f}^{n+1/2} = (f^{n+1} + f^n)/2$ and $\overline{S^*} = (S^* + S^n)/2$, where n stands for the time step and the overbar stands for an averaging operation in time.

The accuracy of the problems in which dispersion is important requires higher order approximation for the linear terms $\partial B/\partial x$ and $\partial S/\partial x$ in Eqs. (4), (5), and (6). Further discussion on dispersion will be given below. Higher order approximation of the derivatives in the nonlinear terms should also be used if the accuracy of the solutions warrants it.

Equations (4) to (6) can be represented in the following finite difference form, with $x = k\,\Delta x$, $t = n\,\Delta t$:

$$(S_k^* - S_k^n)/\Delta t + \overline{S_k^*}\,\mathbf{D}_k A^n/\Delta x + A_k^n\,\mathbf{D}_k S^n/\Delta x + \mathbf{D}_k B^n/\Delta x - \overline{S_k^*}[2U_k^n/r_k\,\mathbf{D}_k S^n/\Delta x + S_k^n\,\mathbf{D}_k(U^n/r)/\Delta x] = 0 \tag{7}$$

$$\begin{aligned}(U_k^{n+1} - U_k^n)/\Delta t &+ (2D_k U_k^n + C^{n+1/2}) \cdot (U_{k+1}^{n+1} - U_{k-1}^{n+1} + U_{k+1}^n - U_{k-1}^n)/(4\Delta x) \\ &- 1/(\Delta t\,\Delta x^2)[(\sigma_{k-1} U_{k-1}^{n+1} - 2\sigma_k U_k^{n+1} + \sigma_{k+1} U_{k+1}^{n+1}) \\ &- (\sigma_{k-1} U_{k-1}^n - 2\sigma_k U_k^n + \sigma_{k+1} U_{k+1}^n)] \\ = &-(1/\Delta x\,\mathbf{D}_k(S^* + S^n)/2 - U_k^n(C_{k+1}^{n+1/2} - C_{k-1}^{n+1/2})/(2\Delta x) - (U_k^n))^2 \\ &\cdot (D_{k+1} - D_{k-1})/(2\Delta x) + 1/\Delta x\,\mathbf{D}_x[(U^n)^2/r(S^* + S^n)/2]\end{aligned} \tag{8}$$

$$(S_k^{n+1} - S_k^n)/\Delta t + S_k^n\,\mathbf{D}_k(A^{n+1} + A^n)/(2\Delta x) + (A_k^{n+1} + A_k^n)/2 \cdot \mathbf{D}_k S^n/\Delta x + (1/\Delta x)\,\mathbf{D}_k(B^{n+1} + B^n)/2 - (1/\Delta x) \cdot \mathbf{D}_k[(S^n)^2/r(U^{n+1} + U^n)/2] = 0. \tag{9}$$

In Eqs. (7), (8), and (9), $(1/\Delta x)\,\mathbf{D}_k P^n$ can be approximated by either one of the following two difference schemes which are accurate to $O(\Delta x^2)$ and $O(\Delta x^4)$ respectively:

Scheme I.

$$\begin{aligned}(1/\Delta x)\,\mathbf{D}_k P^n &= (1/\Delta x) \cdot (P_{k+1}^n - P_{k-1}^n)/2 \\ &= (\partial P^n/\partial x) + (\Delta x^2/6) \cdot (\partial^3 P^n/\partial x^3) + O(\Delta x^4)\end{aligned} \tag{10}$$

Scheme II.

$$\begin{aligned}(1/\Delta x)\,\mathbf{D}_k P^n &= (1/\Delta x)(P_{k-2}^n - 8P_{k-1}^n + 8P_{k+1}^n - P_{k+2}^n)/12 \\ &= (\partial P^n/\partial x) + (\Delta x^4/30) \cdot (\partial^5 P^n/\partial x^5) + O(\Delta x^6).\end{aligned} \tag{11}$$

We shall discuss the implication of the two different schemes below in the section on dispersion.

Equations (7) to (9) can be rearranged to give computational algorithm:

$$\text{(a)} \quad S^* = (1 + \gamma\, \mathbf{D}_k A^n - F_k^n)^{-1} [(1 - \gamma\, \mathbf{D}_k A^n + F_k^n) S_k^n - 2 \cdot \gamma(A_k^n\, \mathbf{D}_k S^n + \mathbf{D}_k B^n)] \tag{12}$$

where $F_k^n = \gamma[2U_k^n/r\, \mathbf{D}_k S^n + S_k^n\, \mathbf{D}_k(U^n/r)]$;

$$\text{(b)} \quad -a_k U_{k-1}^{n+1} + b_k U_k^{n+1} - c_k U_{k+1}^{n+1} = d_k \tag{13}$$

where

$$\begin{aligned}
a_k &= \gamma/2[2D_k U_k^n + C_k^{n+1/2}] + \sigma_{k-1}/\Delta x^2 \\
b_k &= 1 + 2\sigma_k/\Delta x^2 \\
c_k &= -\gamma/2[2D_k U_k^n + C_k^{n+1/2}] + \sigma_{k+1}/\Delta x^2 \\
d_k &= [U_k^n - \gamma/2[2D_k U_k^n + C_k^{n+1/2}]\, \delta_k U^n - 1/\Delta x^2\, \delta_k^2(\sigma U^n) \\
&\quad - \gamma\, \mathbf{D}_k(S^* + S^n) - \gamma U_k^n\, \delta_k C^{n+1/2} - \gamma(U^n)^2\, \delta_k D \\
&\quad + \gamma\, \mathbf{D}_k[(U^n)^2/r(S^* + S^n)]
\end{aligned}$$

$$\text{(c)} \quad S_k^{n+1} = S_k^n - \gamma S_k^n\, \mathbf{D}_k(A^{n+1} + A^n) - \gamma(A_k^{n+1} + A_k^n)\, \mathbf{D}_k S^n - \gamma\, \mathbf{D}_k(B^{n+1} + B^n) + \gamma\, \mathbf{D}_k[(S^n)^2/r(U^{n+1} + U^n)] \tag{14}$$

where $\delta_k f = (f_{k+1} - f_{k-1})$, $\delta_k^2 f = (f_{k-1} - 2f_k + f_{k+1})$, $\gamma = \Delta t/(2\Delta x)$.

In these equations, $\mathbf{D}_k B^n$ and $\mathbf{D}_k S^n$ are either from Scheme I in Eq. (10), or Scheme II in Eq. (11). Equations (12) and (14) are explicit, and (13) is implicit. The latter requires the solution of an $N \times N$ linear system, where N is the number of grid points. Since this linear system has a tridiagonal coefficient matrix, its solution by Gaussian elimination can be done using only $O(N)$ arithmetic operations.

In the computation, we have used $q(t) = Q \cdot \sin(2\pi t/200)$, and set a step-like topography at the origin of a one-dimensional infinite space, $-\infty \leqslant x \leqslant \infty$. If the computation is terminated before the waves reach the boundaries of a computational domain so that no waves are permitted to reflect back into the interior to contaminate the forward propagating solutions, the boundary conditions can be set to either $S = U = 0$, or $\partial S/\partial x = \partial U/\partial x = 0$, or other combination of any two of them at any arbitrary distance $|x| = \mathscr{D}$. If the forcing lasts only for a short period, one can translate the x-axis linearly to allow the wave to propagate indefinitely within a limited computational domain after the forcing has stopped. This procedure is similar to solving the equations along their characteristics and can save a substantial amount of computing time.

4. The Stability Properties

Our experiments show that in the system under investigation, instability occurs some time after the initial pulse has been generated, presumably when the dispersive term of the equation becomes important. Dispersion takes effect very slowly. Its effects are visible only after the initial pulse has travelled some distance away from the step topography. To avoid instability due to abrupt change in water depth, the sharp corners are rounded by putting $r(x) = r_0 + r_1 \tanh \alpha x$. Choosing $\alpha \leqslant 1$ eliminates the topographic instability. We shall investigate the stability properties of the algorithm in a region where there is no topographic gradient, i.e., r_1, r_2, r, and σ are considered to be constants, and $\partial C/\partial x = \partial D/\partial x = 0$. We shall also set $A = aU$ and $B = bU$, $a = (r_2 - r_1)/r$ and $b = r_1 \cdot r_2/r$ being constants, where r_2 and r can be the values at either side of the step. With these approximations, we shall investigate the following model equations:

From (4) we obtain an expression for $\overline{S^*}$ which is then linearized to give

$$\overline{S^*} = 1/\alpha(S^n - \Delta t/2aU_0\, \partial S^n/\partial x - b\, \Delta t/2 \partial U^n/\partial x). \tag{15}$$

Hence

$$\partial \overline{S^*}/\partial x = 1/\alpha(\partial S^n/\partial x - \Delta t/2aU_0\, \partial^2 S^n/\partial x^2 - b\, \Delta t/2 \partial^2 U^n/\partial x^2), \tag{15a}$$

where

$$\alpha = [1.0 + \Delta t/2a\, \partial U_0/\partial x - \Delta t/2(U_0/r\, \partial S_0/\partial x + S_0\, \partial(U_0/r)/\partial x)].$$

The linearized forms of (5) and (6) are

$$(\partial U/\partial t)^{n+1/2} + C_0 \frac{\overline{\partial U}^{n+1/2}}{\partial x} + 2D_0 U_0 \frac{\overline{\partial U}^{n+1/2}}{\partial x} \sigma[\partial(\partial^2 U/\partial x^2)/\partial t]^{n+1/2}$$
$$= -\partial \overline{S^*}/\partial x + U_0^2/r\, \partial S^*/\partial x \tag{16}$$

$$(\partial S/\partial t)^{n+1/2} + a\, \partial U_0/\partial x S^n + aU_0\, \partial S^n/\partial x$$
$$+ b \frac{\overline{\partial U}^{n+1/2}}{\partial x} - 2S_0 U_0/r\, \partial S^n/\partial x = 0. \tag{17}$$

Note that we have obtained (16) and (17) by replacing U and S in (5) and (6) by U_0, and S_0, $\partial B/\partial x$ by $b\partial U_0/\partial x$, and $\partial A/\partial x$ by $a\partial U_0/\partial x$. They represent some typical values of U, S, $\partial B/\partial x$, and $\partial A/\partial x$ from the final solutions. We shall use Scheme I for $\partial/\partial x$ and substitute $\partial S^*/\partial x$ from (15a) into (16), then analyze the stability of the coupled equations (16) and (17).

If we use central differencing for the derivatives and use Fourier representation for the grid point error, i.e., $U_k^n = U^n \exp(ik\, \Delta x)$ and $S_k^n = S^n \exp(ik\, \Delta x)$, where $i = \sqrt{-1}$, then $(\partial U^n/\partial x)_k = i(1/\Delta x) \cdot U^n \cdot \sin k\, \Delta x \cdot \exp(ik\, \Delta x)$, $(\partial^2 U^n/\partial x^2) = (2/\Delta x^2) \cdot U^n(\cos k\, \Delta x - 1) \cdot \exp(ik\, \Delta x) = -U^n[\sin(\Delta x/2)/(\Delta x/2)]^2 \cdot \exp(ik\, \Delta x)$,

where for brevity we have used U^n and S^n to represent their respective computational error at the nth time step. With these substitutions, Eqs. (16) and (17) can be written in matrix form as

$$P\mathbf{X}^{n+1} = Q\mathbf{X}^n, \qquad \mathbf{X} = (U, S)^{\mathrm{T}}, \tag{18a, b}$$

where T stands for the transpose, and P and Q are 2×2 matrices having elements:

$$\begin{aligned}
p_{11} &= [1.0 + \sigma[\sin(\Delta x/2)/(\Delta x/2)]^2] \\
&\quad + i[1/2 \cdot \Delta t/\Delta x \cdot \sin(\Delta x) \cdot (2D_0 U_0 + C_0)] \\
p_{12} &= 0.0 \\
p_{21} &= i[b/2\Delta t/\Delta x \sin(\Delta x)] \\
p_{22} &= 1.0 \\
q_{11} &= (1.0 + [\sigma - \Delta t^2 b/(2\alpha)(1 - U_0^2/r)] \cdot [\sin(\Delta x/2)/(\Delta x/2)]^2) \\
&\quad - i[1/2\Delta t/\Delta x \sin(\Delta x) \cdot (2D_0 U_0 + C_0)] \\
q_{12} &= \Delta t^2/(2\alpha)\, aU_0(U_0^2/r - 1) \cdot [\sin(\Delta x/2)/(\Delta x/2)]^2 \\
&\quad + i\, \Delta t/\alpha(U_0^2/r - 1) \cdot \sin(\Delta x)/\Delta x \\
q_{21} &= -i[b/2\Delta t/\Delta x \sin(\Delta x)] \\
q_{22} &= (1.0 + a\, \Delta t\, \partial U_0/\partial x) + i\, \Delta t \sin(\Delta x)/\Delta x(2S_0 U_0/r_0 - aU_0).
\end{aligned}$$

For stability, we require $|\lambda| < 1.0$, λ being the eigenvalues of $P^{-1}Q$. Before considering the general case, let us first consider the uncoupled equations, i.e., set the off-diagonal elements of P and Q equal to zero. Then the two eigenvalues are

$$\lambda_1 = q_{11}/p_{11}$$

and

$$\lambda_2 = q_{22}.$$

Obviously $|\lambda_1| < 1.0$ for small Δt. Thus the uncoupled, linearized Eq. (16) are unconditionally stable if we neglect the $O(\Delta t^2)$ terms, a well-known property of the implicit procedure. If we keep the $O(\Delta t^2)$ terms, we require $\Delta t < (2\alpha\sigma/[b(1 - U^2/r)])^{1/2}$. The other condition $|\lambda_2| < 1.0$ requires $1.0 > \Delta t \cdot C/\Delta x$, where

$$C = \Delta x/2 \cdot [a\, \partial U_0/\partial x + (\sin(\Delta x)/\Delta x \cdot [2S_0 U_0/r - aU_0])^2/(a\, \partial U_0/\partial x)].$$

Hence the stability of the uncoupled form of Eq. (17) is governed by the CFL criterion of a wave equation with phase speed C.

In order to investigate the coupled equations, we rewrite (18) as

$$\mathbf{X}^{n+1} = P^{-1}Q\mathbf{X}^n = G\mathbf{X}^n, \tag{19}$$

where G is the amplification matrix of the coupled Eqs. (16) and (17). The elements of G are

$$g_{11} = q_{11}/p_{11}$$
$$g_{12} = q_{12}/p_{11}$$
$$g_{21} = -p_{21} \cdot q_{11}/p_{11} + q_{21}$$
$$g_{22} = -p_{21} \cdot q_{12}/p_{11} + q_{22}$$

and its eigenvalues satisfy the following characteristic equation

$$(g_{11} - \lambda)(g_{22} - \lambda) - g_{12} \cdot g_{21} = 0$$

or

$$(q_{11} - \lambda p_{11})(p_{11} \cdot q_{22} - p_{21} \cdot q_{12} - \lambda p_{11}) - q_{12}(p_{11} \cdot q_{21} - p_{21} \cdot q_{11}) = 0. \tag{20}$$

One can readily obtain the two solutions of λ,

$$\lambda = W \pm [W^2 + Z]^{1/2},$$

where

$$W = (q_{11} + p_{11} \cdot q_{22} - q_{21} \cdot q_{12})/2$$
$$Z = (q_{11} \cdot p_{11} \cdot q_{22} - q_{11} \cdot p_{21} \cdot q_{12} - q_{12} \cdot p_{11} \cdot q_{21} + q_{21} \cdot p_{21} \cdot q_{11}).$$

If we neglect $O(\Delta t^2)$ terms, we have the approximate solutions,

$$\lambda_1 = \frac{(1 + m^2\sigma) - i\,\Delta t n c_1}{(1 + m^2\sigma) + i\,\Delta t n c_1} \tag{21a}$$

$$\lambda_2 = \frac{(1 + m^2\sigma)(1 - c_3\,\Delta t) + i\,\Delta t[1 + nc_4(1 + m^2\sigma)]}{(1 + m^2\sigma) + i\,\Delta t n c_1}, \tag{21b}$$

where

$$m = \sin(\Delta x/2)/(\Delta x/2)$$
$$n = \sin(\Delta x)/\Delta x$$
$$c_1 = C_0/2 + D_0 U_0$$
$$c_2 = (1 - U_0^2/r)/a$$
$$c_3 = a\,\partial U_0/\partial x$$
$$c_4 = (2S_0 U_0/r - \alpha U_0).$$

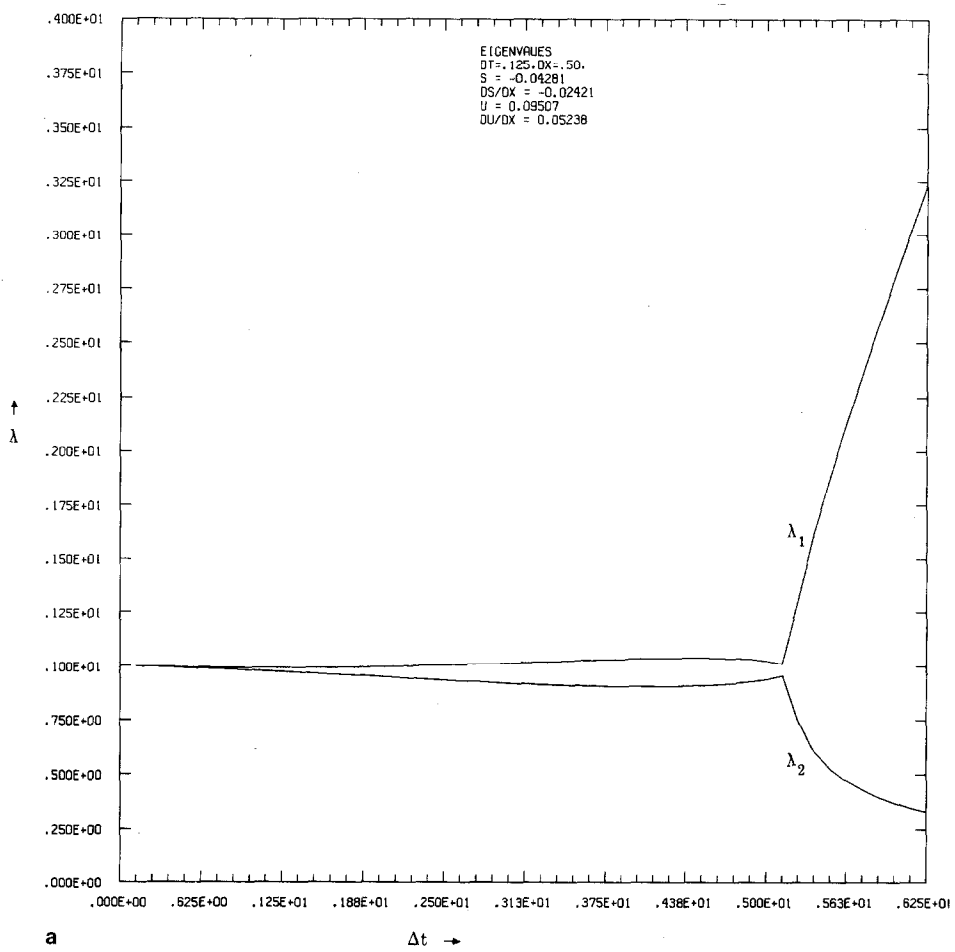

FIG. 2. (a) Absolute eigenvalues of the matrix G as functions of Δt; $S_0 = -0.04281$, $\partial S_0/\partial x = -0.02414$; $U_0 = 0.09507$; $\partial U_0/\partial x = 0.05238$. These are values obtained from the leading wave in shallow water of the computation shown in Figs. 4a and b, with $Q = 0.1$ and $\Delta x = 0.5$. These values are used in the coefficients of the linearized equations for stability analysis. (b) Absolute eigenvalues of the matrix G as function of Δt. The parameters used in the computation are the same as in Fig. 2a except $U_0 = 0$ and $\partial U_0/\partial x = 0$.

Note that m, $n \to 1$ as $\Delta x \to 0$. c_2 is not in λ_1 and λ_2 because the term containing c_2 is $O(\Delta t^2)$. It is obvious that $|\lambda_1| = 1$, and $|\lambda_2| < 1$ if we neglect the $O(\Delta t^2)$ terms.

Therefore the linearized equations are stable if Δt is sufficiently small so that $O(\Delta t^2)$ terms can be neglected. Δx is not a significant contributing factor to instability if, say, it is kept less than unity. However, it is difficult to put a bound on Δt because c_1 to c_4 are all interrelated to the solution of the problem.

In Figs. 2a and 2b, we have plotted the eigenvalues as functions of Δt for given q, U_0, S_0, $\partial U_0/\partial x$, and $\partial S_0/\partial x$ which are obtained from a stable solution. The

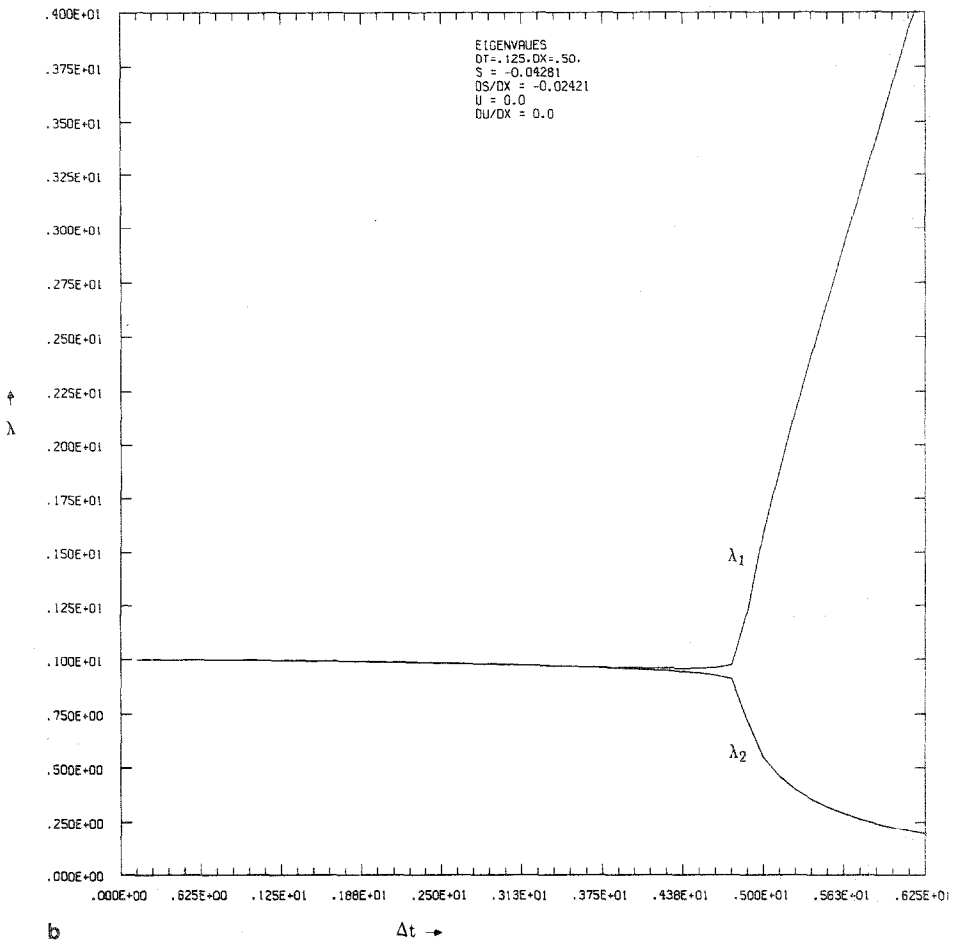

FIG. 2—*Continued*

eigenvalues of G are computed numerically by using the scientific library IMSL [8]. It is clear that from Fig. 2a, $|\lambda_1|$ is increasing and $|\lambda_2|$ is decreasing and both are very close to unity up to $\Delta t = 2.1$ when $|\lambda_1|$ becomes larger than unity. Both eigenvalues change gradually until $\Delta t \approx 5.2$, where they diverge abruptly. We have varied different parameters to see whether or not we can make the two eigenvalues to coalesce. This happens when U_0 and $\partial U_0/\partial x$ are set equal to 0 as shown in Fig. 2b. When S_0 and $\partial S_0/\partial x$ are set equal to zero, the coalescence is not as complete (not shown). Numerical experiments for $Q = 0.1$, $\Delta x = 0.5$, show that $\Delta t = 2.0$ is about the minimum value of Δt at which the numerical system becomes unstable. In general, the Δt used is a great deal smaller than unity in order to maintain accuracy as discussed below. This scheme is therefore extremely robust. It is reassuring that we need not worry about instability when choosing Δt. We must, however, choose

Δt sufficiently small that dissipation will not overwhelm the solutions as we shall [illegible] abruptly. The precise reason for this abrupt divergence has not been established. We speculate that for such large values of Δt, terms containing Δt^2 become dominant in (18), and consequently change the characteristics of the equations. However, such a large value of Δt is outside our interest here.

Our discussion on instability in this section is highly simplified. We have assumed that the shelfbreak itself will not cause any computational difficulty, since we have set $\partial r/dx = 0$ everywhere for the instability analysis. This assumption is certainly true in our studies because we have designed the slope of the shelf to be of order unity, and the shelfbreak has rounded corners as shown below (also see Fig. 1). If the shelf is a true step function with right-angled corners, we may have a different kind of dominant instability limitation.

5. Dissipation

The scheme (12), (13), and (14) can be constructed so that they are non-dissipative. However, when we substitute (15a) into (16) for $\partial \overline{S^*}/\partial x$, we introduce explicitly $O(\Delta t)$ dissipative terms: $\Delta t/2[aU\,\partial^2 S^n/\partial x^2 + b\,\partial^2 U^n/\partial x^2]$. They are independent of Δx and are controllable. Their effects on S are indirect and hence are much more difficult to assess. We shall illustrate the results of numerical dissipation for a computation with $\Delta t = 1.0$, $Q = 0.1$, and $\Delta x = 0.5$. The forcing is applied for half a period. In Table I, column 1 shows the integrated energy over the left half plane, and column 2 shows that over the right half plane at 10 different forcing cycles. The sum of the two is shown in column 3. The dissipation has reduced the wave energy by about 20% over nine forcing cycles on the left half plane, while on the right in deep water, the waves are equilibrating slowly. Thus the dissipative

TABLE I

Energy with $\Delta t = 1.0$ Half Cycle Forcing

Forcing cycle	E_L	E_R	$E_L + E_R$
1	0.1277*E*-01	0.1247*E*-01	0.2524*E*-01
2	0.1277*E*-01	0.1249*E*-01	0.2526*E*-01
3	0.1279*E*-01	0.1253*E*-01	0.2532*E*-01
4	0.1277*E*-01	0.1259*E*-01	0.2535*E*-01
5	0.1250*E*-01	0.1264*E*-01	0.2515*E*-01
6	0.1206*E*-01	0.1269*E*-01	0.2475*E*-01
7	0.1161*E*-01	0.1274*E*-01	0.2435*E*-01
8	0.1123*E*-01	0.1279*E*-01	0.2401*E*-01
9	0.1089*E*-01	0.1284*E*-01	0.2373*E*-01
10	0.1059*E*-01	0.5112*E*-01	0.1570*E*-01

TABLE II

Energy with $\Delta t = 0.125$ Half Cycle Forcing

Forcing cycle	E_L	E_R	$E_L + E_R$
1	0.1279*E*-01	0.1247*E*-01	0.2526*E*-01
2	0.1279*E*-01	0.1249*E*-01	0.2528*E*-01
3	0.1282*E*-01	0.1252*E*-01	0.2533*E*-01
4	0.1288*E*-01	0.1255*E*-01	0.2543*E*-01
5	0.1294*E*-01	0.1258*E*-01	0.2551*E*-01
6	0.1296*E*-01	0.1260*E*-01	0.2555*E*-01
7	0.1295*E*-01	0.1261*E*-01	0.2556*E*-01
8	0.1293*E*-01	0.1262*E*-01	0.2555*E*-01
9	0.1290*E*-01	0.1263*E*-01	0.2553*E*-01
10	0.1286*E*-01	0.5068*E*-01	0.1793*E*-01

effects are different in shallow and deep waters. The reasons are as follows: the coefficients a and b in the numerical dissipative terms in Eq. (15a) are proportional to $1/r$. Hence they are larger in shallow water, where r is small, than that in deep water. Another effect is more indirect. Since the physical dispersion coefficient is proportional to $r_1 \cdot r_2$, dispersion is larger in deep water than in shallow water. We shall show later that within a wave train which contains a constant amount of energy, the larger the dispersion, the longer are the waves within the wave packet, or the smaller the wave number, k. Since dissipation is proportional to k^2, it is therefore larger in the shallow water. For comparison, we also give the integrated energy for a similar computation with $\Delta t = 0.125$ in Table II. As we can see, the dissipation is negligibly small for $\Delta t = 0.125$, and $Q = 0.1$. The energy has been computed from the formulae

$$E_L = \int_{-\mathscr{D}}^{0} \eta(S, U, x)\, dx = \sum_{j=-J}^{0} \eta(S_j, U_j, x_j)\, \Delta x$$

$$E_R = \int_{0}^{\mathscr{D}} \eta(S, U, x)\, dx = \sum_{0}^{j=J} \eta(S_j, U_j, x_j)\, \Delta x,$$

where

$$\eta(S, U, x) = 1/2[S^2 + (r_1 - S)(r_2 + S)/r \cdot U^2 + 1/(3r)(r_1 \cdot r_2 \cdot \partial U/\partial x)^2]. \quad (22)$$

The integrals over $-\mathscr{D} \leqslant x \leqslant \mathscr{D}$ are approximated by Simpson's rule.

6. Dispersion

Dispersion arises from derivatives of third order in x or in t, or from mixed derivatives such as the term $\partial^3(\sigma U)/\partial t\, \partial x^2$ in Eq. (2). In the finite difference

formulation of the equations, third-order derivatives can be inadvertently introduced as truncation errors in second-order approximations of the first-order derivatives. For example, the approximation of the time derivative,

$$(f^{n+1}-f^n)/\Delta t=(\partial f//\partial t)^{n+1/2}+(\Delta t^2/24)(\partial^3 f/\partial t^3)^{n+1/2},$$

introduces an $O(\Delta t^2)$ numerical temporal dispersion. This can be eliminated only if we use a three- or multiple-leveled schemes, whose advantage, however, is not overwhelming [4]. In order to keep this numerical dispersion from contaminating the physical dispersion, we have to keep Δt small. In practice, the dissipative effect due to large Δt is much more worrisome than dispersion. Similarly, the approximation of the first order spatial derivatives, including those in the nonlinear terms, can also introduce numerical dispersion. For our computations, the nonlinear terms are sufficiently small that we need not worry about dispersion due to their truncation errors. On the other hand, linear terms $\partial B/\partial x$ and $\partial S/\partial x$ in Eqs. (1) and (2) need special treatment. While using Scheme I in Eq. (10) to approximate these terms will introduce an $O(\Delta x^2)$ dispersion terms, Scheme II in Eq. (11) gives only on $O(\Delta x^4)$ truncation error.

In Figs. 3a and 3b, we compare the results of three separate computations with the combination of different Δt and Scheme I or II. In all these computations, the forcing function $q(t)=0.1\sin(2\pi t/200)$ for $0<t<100$, $q(t)=0$ for $t>100$, and $\Delta x=0.5$ are used. The solid dots in Fig. 3 represent the analytical solitary wave solution which satisfies Eqs. (1) and (2) when $q(t)=0$ and $r(x)=$constant. The leading waves of the numerical solutions are expected to be accurately represented by this solution.

Curves 1 in Figs. 3a and b use $\Delta t=0.125$ and Scheme II for all the spatial derivatives denoted by D_k in Eqs. (7), (8), and (9). These curves are very accurate when compared with the theoretical values (solid dots). It seems that $\Delta t=0.125$ is sufficiently small to suppress numerical dissipation and dispersion for this computation. The discrepancy between theory and computation at the trailing edge of curve 1 shown in Fig. 3a is due to the influence of the wave following directly behind. It is expected that at large time when the leading wave has separated from the rest of the wave train, the analytical and numerical solutions will agree even better.

Curve 2 in Fig. 3a uses Scheme I for the linear terms $\partial B/\partial x$ and $\partial S/\partial x$, and $\Delta t=0.125$. Curve 2 is significantly wider than curve 1. In fact the former fits a solitary wave for a substantially different dispersion coefficient, σ. If we consider a solitary wave of the form $\operatorname{sech}^2[k(x-ct)]$, then σ is proportional to $1/(k^2)$. Fitting curve 2 into this wave form gives $k=0.4$ instead of the correct value $k=0.6$, which is the appropriate value for curve 1. Thus using Scheme I for the linear terms has increased the effective dispersion by a factor of more than 2.

Curve 3, which uses Scheme II for D_k and $\Delta t=1.0$, represents the solution at the same evolutionary time as curves 1 and 2. Curve 4 is the same wave five forcing cycles earlier. Note the significant reduction in amplitude and in width in curve 3 when compared with curve 1. The reduction in amplitude is due to the increase in

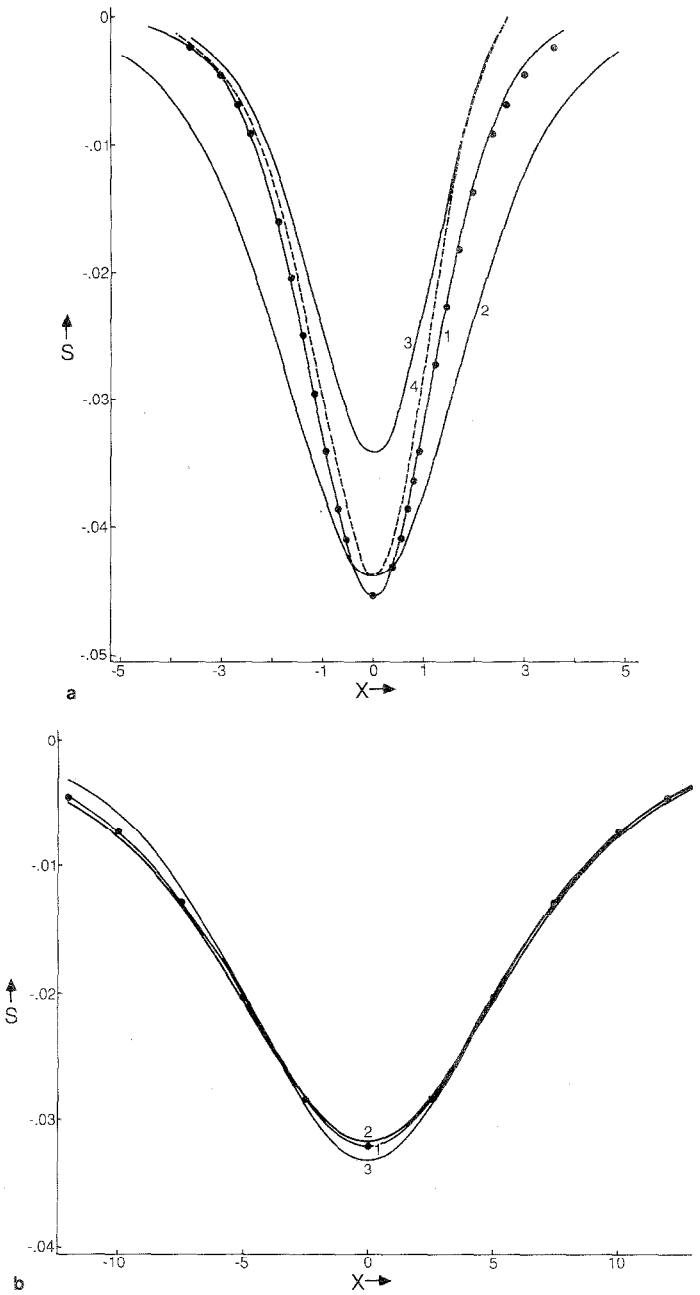

FIG. 3. (a) Comparison of the elevation S of the leading wave in the solitary wave train in the shallow water. Curve 1 is for $\Delta t = 0.125$, all first order spatial derivatives being represented by Scheme II. Curve 2 is for a model whose parameters are the same as those for curve 1 except the linear terms in Eqs. (6), (7), and (8) are approximated with Scheme I. Curve 3 is for $\Delta t = 1.0$. Other parameters are the same as curve 1. Curves 1, 2, and 3 represent the leading wave at the end of the 10th forcing period. Curve 4 is at the end of the 5th period for $\Delta t = 1.0$, or it represents the same wave as curve 3 at an earlier time. (b) Comparison of the leading wave of the solitary wave train in deep water at the end of the 9th forcing period. See the caption of Fig. 3a for details.

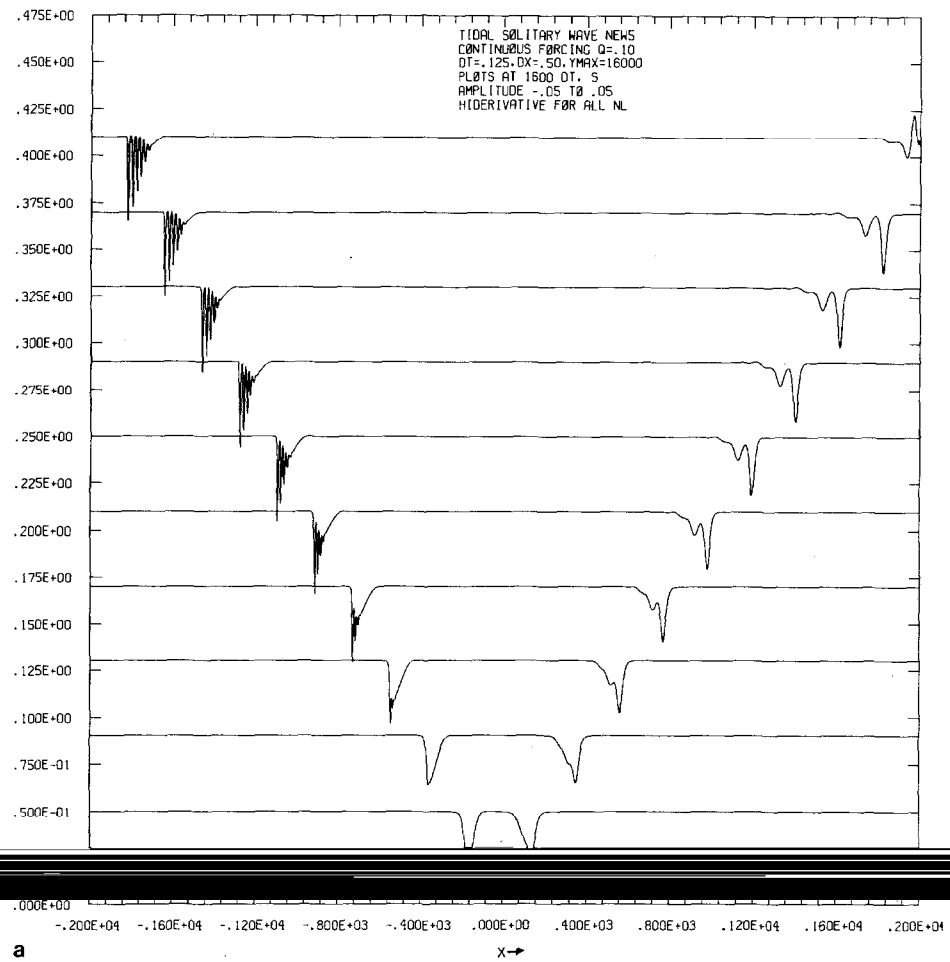

FIG. 4. (a) The elevation S of solitary wave trains computed with Scheme II; $\Delta t = 0.125$, $\Delta x = 0.5$. Forcing function $q(t) = 0.1 \sin(2\pi t/200)$ for $t \leqslant 100$, and $q(t) = 0$ for $t > 100$. Note the differences in wave forms and phase speeds in both the shallow and in deep water. The curves are plotted with a separation of 1 forcing period, from period 1 to 10. The time progresses from the bottom to the top graph. The ordinate scale is the true scale for the displacement of S. Each curve should start from zero in the ordinate. (b) The shear U of the solitary wave trains. See caption of Fig. 4a for details of explanation.

dissipation for large Δt, and the reduction in width is due to decrease in dispersion (opposite to curve 2). In Fig. 3b, all curves are bundled together much closer than those in Fig. 3a. This shows that in deep water, the effects of the truncation errors are less severe.

We can conclude from these comparisons that: (1) numerical dissipation due to large Δt has reduced the wave amplitude by more than 20% as shown in the

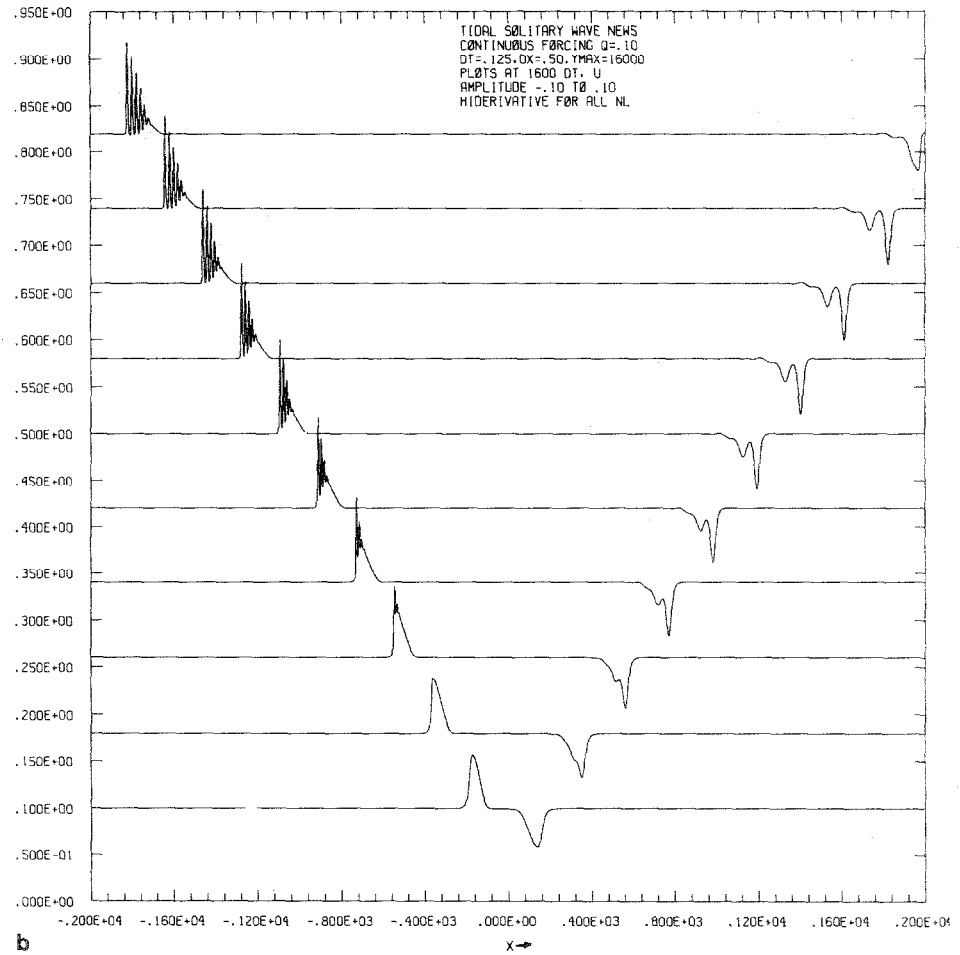

FIG. 4—*Continued*

difference between curve 3 and curve 2; (ii) the numerical dispersion due to the $\partial^3 S/\partial t^3$ truncation term works in the opposite direction of the spatial numerical dispersion as shown in curve 2 (excessive spatial dispersion) and curve 3 (excessive temporal dispersion, opposite in sign); and (iii) in deep water as shown in Fig. 3b, numerical dissipation and dispersion are much less severe than in shallow water. Numerical experiments have also shown that using Scheme I for the nonlinear terms does not change the solutions appreciably. Furthermore, second-order spatial approximations for the first-order derivatives in an implicit scheme as in Eq. (5) does not affect the solutions very much, presumably because solutions obtained from an implicit scheme are spatially more consistent with the equation than those from an explicit scheme. Thus the effects of the truncation errors are reduced.

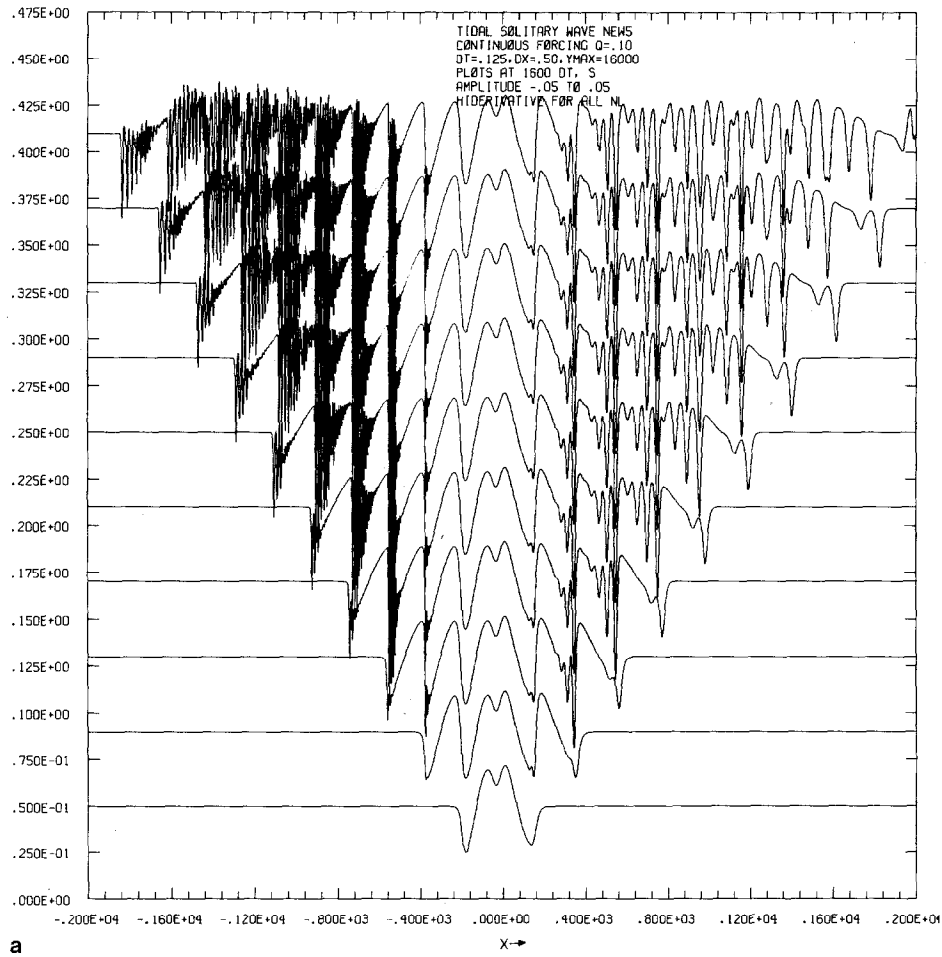

a

FIG. 5. (a) The elevation S of a solitary wave train with continuous forcing, $q(t) = 0.1 \sin(2\pi t/200)$ for $t > 0$. For details explanation see caption of Fig. 4a. (b) The shear U of a solitary wave train with continuous forcing. For details see captions of Figs. 5a and 4a.

7. SAMPLE RESULTS

We shall present the results of two sample computations here. Both computations are for $\Delta t = 0.125$, $\Delta x = 0.5$, $r_1 = 0.25$, $r(x) = [10.5 + 9.5 \tanh(x/10)]$. Therefore $r(x)$ is a step function at $x = 0$ with rounded corners as shown in Fig. 1; $r(x) \to 1.0$ as $x \to -\infty$ and $r(x) \to 20.0$ as $x \to \infty$. The e-folding distance for the rounded corners is 10.0 nondimensional spatial units from the shelfbreak, and the slope is $O(1)$ at $x = 0$. The forcing of the two cases are $q(t) = Q \cdot \sin(2\pi t/200)$, with $Q = 0.1$. Thus the cyclic forcing has a period of 200 nondimensional time units, or 1600 time steps. For case 1, the forcing is $q(t)$ for $0 < t \leqslant 100$, and zero for $t > 100$. Therefore, the

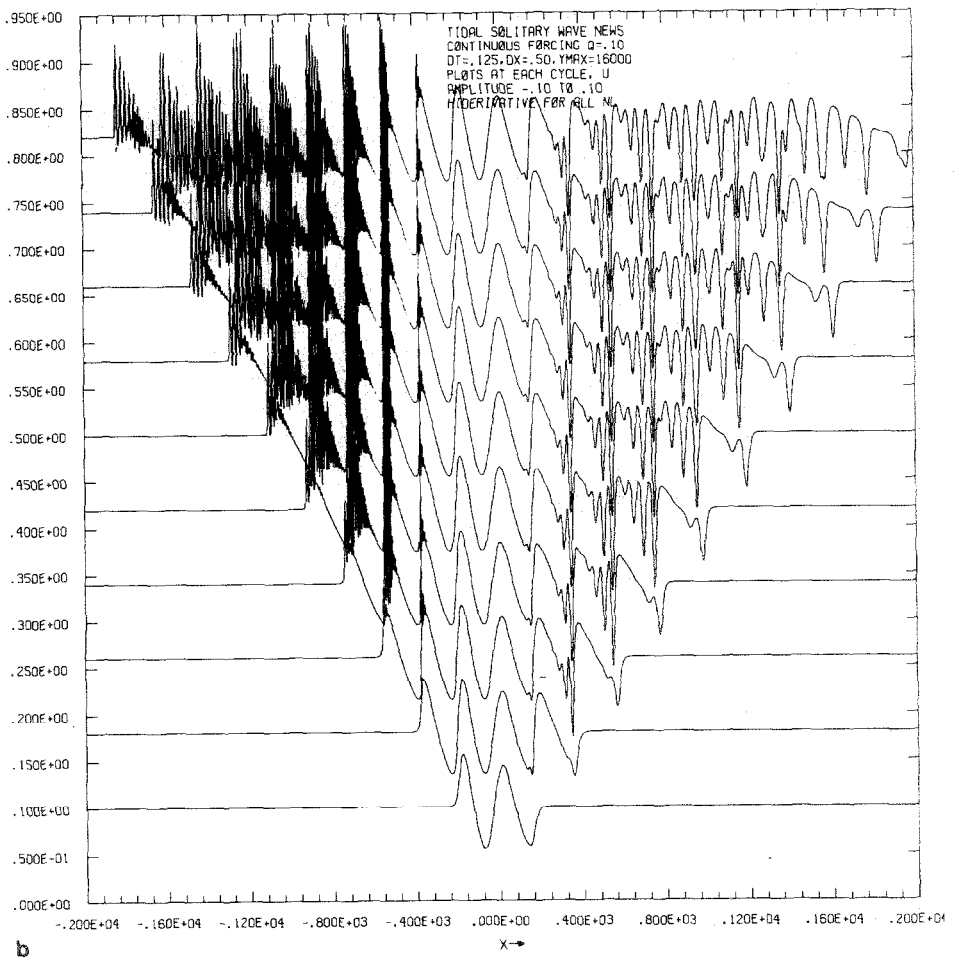

FIG. 5—*Continued*

forcing lasts for one-half of a cycle. Case 2 has a continuous forcing, $q(t)$, for $t > 0$. Computations are stopped after 10 complete periods, or after a nondimensional time lapse of 2000 units.

Figures 4a and b show the amplitude S and shear U of case 1 with sinusoidal forcing for half a period. Figures 5a and b show those of case 2 with continuous periodic forcing. The waves propagate away from the center to both the left and the right direction. The time lapse between each horizontal line is one period of forcing time. The time progresses from bottom to the top. The total horizontal distance is 4000 Δx or 2000 dimensionless units (recall that the depth of the shelf is unity).

The difference between the wave forms on either side of the step arises from the difference in the total water depth. As a result, the dispersion in the deep water side is $19.75/\cdot 75 \approx 26.33$ times as large as that on the shelf. Note that the top lines show

that the wave trains on the right have hit the boundary. This is reflected in the energies in Tables I and II.

There are also differences between the waves in Fig. 5 and those in Fig. 4 at any distance from the shelf break. This is mainly due to the nonzero background flow $q(t)$ for case 2 in Fig. 5. These differences can be explained theoretically as given in a sequel paper [12].

8. Discussion

The finite difference scheme we have presented in this paper is very robust. Although the spectral method is more accurate [5, 6], the finite difference method is much simpler to use, especially when we introduce arbitrary topography and irregular time dependent forcing obtained from observation in the future. It is this versatility that prompted us to choose this avenue of investigation. We have found that the spatial numerical dispersion must be properly controlled by using higher order approximation for the first-order spatial derivatives. The $O(\Delta t)$ dissipation is inherent in this scheme and cannot be eliminated. We have also found that $\Delta t = 0(0.1)$ is sufficiently small to give accurate numerical results in our computations. An alternative method to represent accurately the first- and second-order spatial derivatives is by using cubic spline [1, 2]. This procedure is, however, more complicated than the method we have described here and is presently under investigation.

References

1. J. H. Ahlberg, E. N. Nilson, and J. L. Walsh, *The Theory of Splines and Their Applications* (Academic Press, New York, 1967).
5. B. Fornberg and G. B. Whitham, *Philos. Trans. Roy. Soc. London Ser. A* **289**, 373 (1978).
6. D. Gottlieb and S. A. Orszag, *Numerical Analysis of Spectral Methods: Theory and Application* (SIAM, Philadelphia, 1977).
7. B. Y. Guo and W. M. Cao, *J. Comput. Phys.* **74**, 110 (1988).
8. IMSL, (Int. Math. Statist. Library, Houston, 1984).
9. A. Jeffrey and T. Kakutani, *SIAM Rev.* **14**, 582 (1972).
10. R. M. Mirie and C. H. Su, *J. Fluid Mech.* **115**, 475 (1982).
11. D. H. Peregrine, *J. Fluid Mech.* **25**, 321 (1966).
12. H. Sandstrom and C. Quon, *J. Fluid Mech.*, (submitted and under revision).
13. A. C. Vliegenthart, *J. Eng. Math.* **5**, 137 (1971).
14. G. B. Whitham, *Linear and Nonlinear Waves* (Wiley, New York, 1974).
15. N. J. Zabusky and M. D. Kruskal, *Phys. Rev. Lett.* **15**, 240 (1965).
16. Q. Zou and C. Su, *Phys. Fluids* **29**, 2113 (1986).